NUCL SCI TECH (2017) 28:47
DOI 10.1007/s41365-017-0206-y

How crystal configuration affects the position detection accuracy in pixelated molecular SPECT imaging systems?

Hojjat Mahani[1,2] · Gholamreza Raisali[1] · Alireza Kamali-Asl[3] · Mohammad Reza Ay[2,4]

Received: 17 February 2016 / Revised: 8 June 2016 / Accepted: 11 July 2016

Abstract It is well known that inter-crystal scattering and penetration (ICS–P) are major spatial resolution limiting parameters in dedicated SPECT scanners with pixelated crystal. In this study, the effect of ICS–P on crystal identification in different crystal configurations was evaluated using GATE Monte Carlo simulation. A ^{99m}Tc pencil-beam toward central crystal element was utilized. Beam incident angle was assumed to vary from 0° to 45° in 5° steps. The effects of various crystal configurations such as pixel-size, pixel-gap, and crystal material were studied. The influence of photon energy on the crystal identification (CI) was also investigated. Position detection accuracy (PDA) was defined as a factor indicating performance of the crystal. Furthermore, a set of ^{99m}Tc point-source simulations was performed in order to calculate peak-to-valley (PVR) ratio for each configuration. The results show that the CsI(Na) manifests higher PDA than NaI(Tl) and YAP(Ce). In addition, as the incident angle increases, the crystal becomes less accurate in positioning of the events. Beyond a crystal-dependent critical angle, the PDA monotonically reduces. The PDA reaches 0.44 for the CsI(Na) at 45° beam angle. The PDAs obtained by the point-source evaluation also behave the same as for the pencil-beam irradiations. In addition, the PVRs derived from flood images linearly correlate their corresponding PDAs. In conclusion, quantitative assessment of ICS–P is mandatory for scanner design and modeling the system matrix during iterative reconstruction algorithms for the purpose of resolution modeling in ultra-high-resolution SPECT.

Keywords Monte Carlo · GATE · Molecular SPECT · Position detection accuracy · Pixelated crystal

1 Introduction

Small-animal SPECT imaging becomes an increasingly leading technology in both preclinical molecular imaging and biomedical small-animal studies in the field of radiopharmaceutical development and cancer research [1]. To study functional information in a molecular perspective, a dedicated SPECT instrument is needed [2]. Pixelated SPECT systems are preferred for small-field-of-view configurations [3]. The pixelated crystal limits the degree to which scintillation light spreads laterally and therefore can improve spatial resolution in comparison with a camera that use continuous crystals [4]. However, inter-crystal scattering causes mispositioning of scintillation events, which is of particular concern in imaging detectors based on small discrete scintillator elements [5]. Calculation of the ICS–P is of special importance in pinhole (or slit-hole) collimators where the photons may reach the detector with a considerable oblique angle. In other words, photons

This work was supported by Research Center for Molecular and Cellular Imaging (RCMCI), Tehran University of Medical Sciences (No. 29885).

✉ Mohammad Reza Ay
mohammadreza_ay@sina.tums.ac.ir

[1] Radiation Application Research School, Nuclear Science and Technology Research Institute, Tehran, Iran

[2] Research Center for Molecular and Cellular Imaging, Tehran University of Medical Science, Tehran, Iran

[3] Radiation Medicine Department, Shahid Beheshti University, Tehran, Iran

[4] Department of Medical Physics and Biomedical Engineering, Tehran University of Medical Science, Tehran, Iran

Published online: 27 February 2017

originating from a source at edge of the filed-of-view (FOV) of the camera can introduce a high value of ICS–P.

Thus far, there are limited numbers of studies investigating effect of ICS–P in molecular SPECT cameras. Rasouli et al. [6] investigated effects of ICS–P on detection efficiency of a dedicated breast gamma camera. In 2011, Adibpour et al. [7] studied such effects in a small-animal gamma camera. Zeraatkar and co-workers assessed ICS–P events for a PET scanner, in 2011 [8]. A comprehensive work was conducted by Ghazanfari et al. [9] to assess the effects of crystal material and size on performance of a rotating-head PET scanner, in 2012.

The primary objective of the current study was to investigate possible effects of crystal configuration on position detection accuracy (PDA) in small-animal SPECT cameras using accurate GATE Monte Carlo (MC) simulations. The current research not only studied the effect of the crystal pixel-size and material, but also assessed the influence of pixel-gap and photon energy on the PDA, which is also known as crystal identification (CI). In other words, we aimed to quantitatively assess the impacts of inter-crystal scattering and penetration (ICS–P) on CI in high-resolution molecular SPECT imaging.

2 Materials and methods

In this section, simulation geometry, GATE Monte Carlo study, our assessment strategy based upon PDA, and finally validation of the simulations are comprehensively described.

2.1 Simulation geometry

2.1.1 Pencil-beam simulations

A schematic geometry used to evaluate the effects of ICS–P is illustrated in Fig. 1. A pencil-beam of ^{99m}Tc irradiating central crystal element in combination with a section of the pixelated crystal are also shown. In order to assess the PDA, the collimator was deliberately removed, and PDA was quantified in various array configurations.

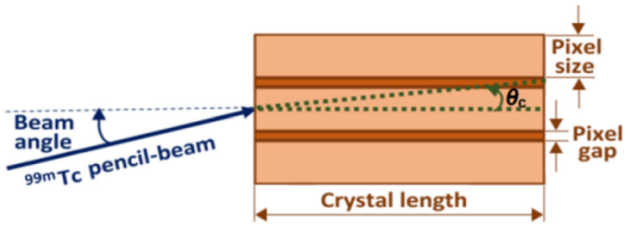

Fig. 1 Schematic view of the simulation geometry including a pencil-beam of ^{99m}Tc along with side view of three crystal pixels

To model oblique gamma rays facing the crystal, the pencil-beam was angled respecting normal vector of the crystal surface. Theoretically, there is a critical angle, above which the incident beam can enter an adjacent crystal pixel, leading to an increase in contribution of neighbor pixels in radiation detection process. Such an angle is geometry dependent and can be fully determined by crystal pixel-size and pixel-gap. The critical angle, θ_c, can be expressed as follows:

$$\theta_c = \tan^{-1}\frac{(0.5s+g)}{l}, \quad (1)$$

where s is the pixel-size, g is the pixel-gap, and l is the crystal length (fixed to 5 mm).

2.1.2 Point-source simulations

In real SPECT systems, the neighbor crystals are simultaneously irradiated as well. To take the contribution of these neighbor crystals in PDA into account, a set of point-source simulations was conducted for various CsI(Na)-based crystal configurations. For this, an 11 × 11 CsI(Na) crystal array was irradiated by a ^{99m}Tc point-source located at a 60-mm source-to-crystal distance, and then the PDA was assessed. It should be noted that the collimator was removed.

2.2 Monte Carlo study

Monte Carlo methods are extensively used in nuclear medicine to assist in the design of new medical imaging devices [10]. GATE combines advantages of GEANT4 simulation toolkit with original features to emission tomography [11]. MC simulations allowed us to assess those parameters (e.g., the ICS–P) which cannot be experimentally measured.

Dead time of the crystal material and half-life of the radiotracer were taken into account in the MC simulations. Particle interactions simulated include photoelectric, Compton scattering, electron ionization, multiple scattering, and bremsstrahlung. Moreover, a 20% energy window centered at the photopeak was applied to the simulated data. In addition, two glass position-sensitive photomultiplier tubes (PS-PMTs) were modeled as back-scattering media behind the pixelated crystal.

2.3 Assessment strategy

2.3.1 Pencil-beam simulations

The GATE MC code was then used for detailed transport of ^{99m}Tc photons originated from a pencil-beam toward the central pixel of the simulated geometry. Multiple simulations at different gamma-ray angles of

incidence were performed, in order to investigate the effects of photon angle on ICS and penetration (parallax) phenomena. The beam angles varied from 0° to 45° (5° steps) respecting normal vector of the crystal.

PDA, the ratio of detected photons in irradiated crystal to the total detected events, was defined, indicating how accurate is the signal positioning when a ^{99m}Tc photon reaches with an oblique angle. On the other hand, in the absence of the collimator, the MC simulations could be dramatically shortened. Also, in an ideal imager, a PDA of unity would be expected.

The PDA was calculated for three common crystal materials, i.e., CsI(Na), NaI(Tl), and YAP(Ce), and various geometrical configurations of the crystal at a fixed crystal thickness of 5 mm. The pixel-size ranged from 0.5 mm × 0.5 mm to 2 mm × 2 mm (0.5-mm steps). In addition, pixel-gap was assumed to be 0.1, 0.2, and 0.3 mm of epoxy. Moreover, it was worth calculating the effect of photon energy on PDA quantification with ^{99m}Tc, ^{111}In, and ^{131}I as low-, medium-, and high-energy tracers, respectively.

2.3.2 Point-source simulations

In the case of point-source evaluation, the PDA was redefined as follows: The ratio of the total number of photons reached all individual crystals and detected in the same crystals to the total detected counts. We note that such a definition would also be valid for the pencil-beam data and results in the same PDA values. This re-definition includes contribution of the neighbor pixels in calculating the PDA for different CsI(Na)-based configurations as for the pencil-beam simulations.

The point-source simulation also allows to study flood images by calculating peak-to-valley ratios (PVRs) using a line-profile of the images. The PVR well reflects crystal identification in pixelated detectors. In order to calculate the PVRs, spatial uncertainties in position estimation caused by the two PS-PMTs as well as our positioning-circuit are modeled as a 2D Gaussian function. Convolving the detector response with the 2D Gaussian function emulates the integrated effect of the PS-PMTs and the positioning-circuit, since we are extracting the PVRs from MC simulations. In order to mimic a more realistic SPECT simulation, electronic noise is added to the calculated flood images. However, this procedure neglects deteriorations in response at edges of the detection module commonly caused by the PS-PMTs readings.

2.4 Simulation validation

We validated our GATE MC simulation procedure against the experimental data acquired by using HiReSPECT, a dual-headed high-resolution small-animal SPECT camera benefited from pixelated CsI(Na) crystal [12–14]. Spatial resolution of the camera for a ^{99m}Tc point-like source in different source-to-collimator distances (SCDs) was then evaluated. Full-width-at-half-maximum (FWHM) of corresponding point-spread-function (PSF) was considered as spatial resolution. The experiments were conducted at conditions as for our GATE simulations.

3 Results and discussion

3.1 Simulation validation

Figure 2 compares MC calculated spatial resolutions with those obtained in our experiments using the HiReSPECT system across several SCDs. CsI(Na) is the crystal material, and crystal configuration is a 1 mm × 1 mm pixel-area with 0.2 mm epoxy separator array. Since the modeled scanner is a dual-headed gamma camera, the FWHM values have been averaged. The simulation and experiment results show good agreement (maximum ∼8% difference at collimator face), and spatial resolution (FWHM) of the HiReSPECT camera increases linearly with SCD.

3.2 Pencil-beam simulations

3.2.1 Crystal material

PDA over all beam angles for 1 mm × 1 mm pixel-area and 0.2 mm epoxy separator, with three common crystal materials of CsI(Na), NaI(Tl), and YAP(Ce) is plotted in Fig. 3. One sees that PDA decreases with increasing incident angles. The CsI(Na) crystal indicates the higher PDA over all beam angles than the NaI(Tl) and YAP(Ce) types. Indeed, CsI(Na) possesses the highest linear attenuation coefficient among the three crystals [15], hence the highest probability of 140 keV photons detection, and a higher CI (i.e., the PDA). The CsI(Na) is benefited from a lower cost and higher light output, as well [16].

For better visualization, only a portion of the crystal is plotted.

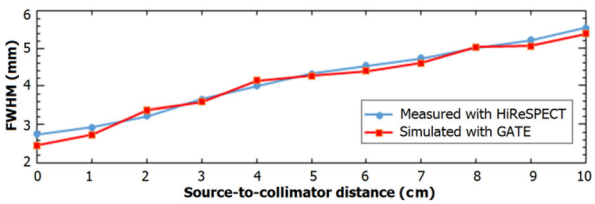

Fig. 2 Simulation and measurement results of spatial resolution of the HiReSPECT at different SCDs

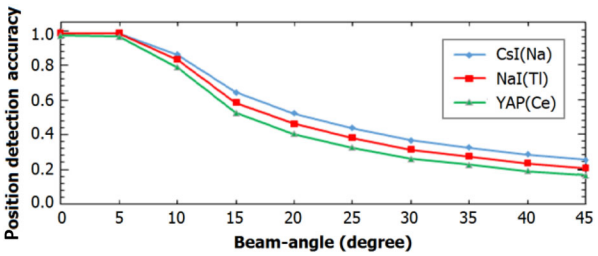

Fig. 3 Position detection accuracy versus beam angle for a 1 mm × 1 mm pixel-area and 0.2 mm epoxy gap configuration with different crystal materials

Figure 4 illustrates scatter plots of the detected counts for a 1 mm × 1 mm pixel-area and 0.2 mm epoxy separator array at 0° and 45° incidence. Contribution of adjacent crystals in detection process is shown in Fig. 4b. The red arrows indicate registered counts in the irradiated crystal. We noted that only a portion of the pixelated crystal is depicted, for better visualization.

Considering a photon arrives at the crystal with an oblique angle. This photon may be geometrically entered an adjacent pixel without any interaction and can be detected in another element rather than the irradiated one. At this condition, a mispositioning of the signal occurs, leading to a decreased PDA. As the incident angle increases, the problem becomes more rigorous. We limited our investigations to a maximum incident angle of 45° because a photon with an incident angle greater than such a limit may passed through multiple collimator septa, and this is practically impossible due to high photoelectric cross section of the collimator material (i.e., lead) at 140 keV.

3.2.2 *Crystal pixel-size*

Figure 5 provides a plot comparing PDAs for four pixel-sizes ranging from 0.5 mm × 0.5 mm to 2 mm × 2 mm all for a 0.2-mm epoxy gap. The PDA increases with the crystal pixel dimension for a given fixed epoxy separator. Figure 5 proves that the higher the crystal pixel-sizes, the higher the PDA, because the ^{99m}Tc photons travel longer distances in the same crystal element and therefore have higher likelihood to be detected in the element at oblique angles. In other words, increasing the crystal pixel-size reduces fraction of those photons experienced ICS–P and detected in neighbor elements. For example, the PDA drops from 0.44 to 0.14 when the pixel-size reduces from 2 mm × 2 mm to 0.5 mm × 0.5 mm, respectively. Although, from Fig. 1, crystal length can control CI in the same manner, but in this study we assumed a fixed-length (i.e., 5 mm) crystal configuration. Figure 5 is also an evident that increasing the pixel-size consequently increases the critical angle.

For 1 mm × 1 mm pixel-area and 0.2 mm epoxy separator crystal geometry, Fig. 6 shows the percentage of detected photons in one adjacent pixel of the irradiated element for the CsI(Na), which is useful for investigating parallax artifact. As the photon incident angle is getting greater (beyond the critical angle), the counts in the adjacent pixel significantly increase so that the beam entirely passes the adjacent pixel, a second critical angle (for example, 20° for 1 mm × 1 mm pixel-area and 0.2 mm gap configuration). Further increasing the incident angle results in fewer counts, because the next neighbor is now involved in detecting the 140 keV primary photons.

3.2.3 *Crystal pixel-gap*

The influence of the epoxy gap between crystals as a function of beam angle for pixel-gaps of 0.1, 0.2, and 0.3 mm is revealed in Fig. 7a, for 1 mm × 1 mm pixel-area configuration. As for the pixel-size, the pixel-gap behaves as the same manner. Figure 7b compares PDA values of various CsI(Na) crystal configurations at 45° incident angle. The positioning accuracy increases with either pixel-size or pixel-gap.

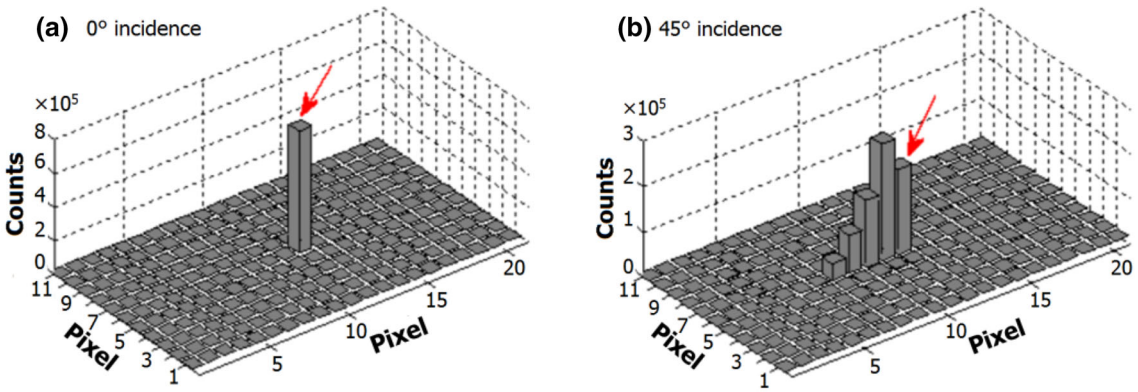

Fig. 4 Scatter plot of the detected photons at 0° and 45° incident angle, for a 1 mm × 1 mm pixel-area and 0.2 mm epoxy configuration

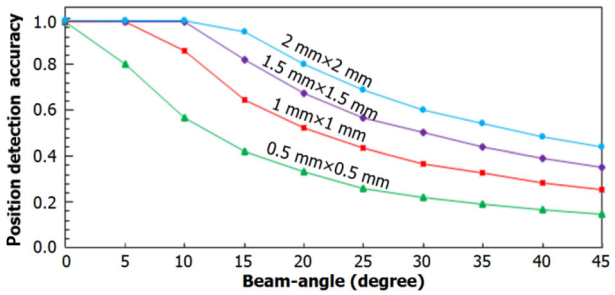

Fig. 5 Position detection accuracy versus beam incident angle for pixel-sizes of 1 mm × 1 mm to 2 mm × 2 mm, at 0.2 mm epoxy gap

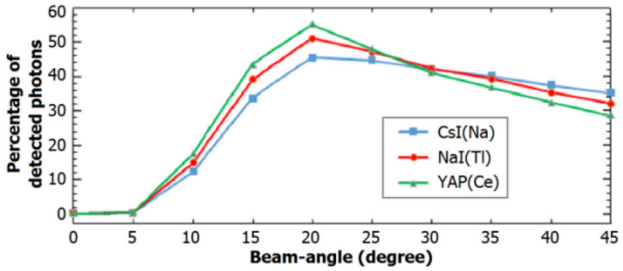

Fig. 6 Percentage of the detected photons in an adjacent pixel for a 1 mm x 1 mm pixel-area and 0.2 mm pixel-gap configuration with different materials

Likewise, as the pixel-gap increases, a ^{99m}Tc photon has a higher probability to be attenuated within the epoxy separator, therefore resulting in lesser counts in an adjacent pixel. In addition, more light photons produced within the crystal element were reflected off the pixel-gap. Quantitatively, a maximum reduction of 13% in the PDA occurs when the pixel-gap varies from 0.3 mm to 0.1 mm for a 1 mm × 1 mm pixel-area crystal configuration. However, influence of pixel-size on the PDA is more severe than of pixel-space, as it is evident from Fig. 5. As can be understood from the results, below the critical angles, for example, 8° for a 1 mm × 1 mm pixel-area and 0.2 mm gap geometry, quantitative variations of the detected photons are negligible and beyond such critical angles, the PDA falls dramatically off.

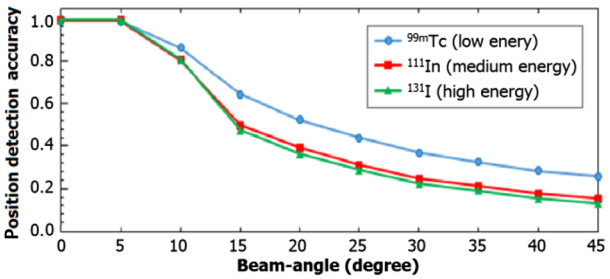

Fig. 8 Position detection accuracy for ^{99m}Tc, ^{111}In, and ^{131}I, with CsI(Na) crystal of 1 mm × 1 mm pixel-area and 0.2 mm epoxy gap

3.2.4 *Photon's energy*

Figure 8 shows how probe's energy affects the CI for 1 mm × 1 mm pixel-area and 0.2 mm epoxy gap CsI(Na) configuration. Three probes of ^{99m}Tc, ^{111}In, and ^{131}I were used. As can be observed, the PDA decreases with increasing energy, due to an increase in scattered and penetrated components in the detected signal. In more details, the CsI(Na) crystal owns mass attenuation coefficients of 0.990, 0.291, and 0.144 cm^2 g^{-1} at 140, 245, and 364 keV, respectively [15]. Therefore, a lower-energy SPECT probe automatically leads to a more accurate SPECT imaging from CI point of view. In other words, the parallax artifact is more serious when a high-energy SPECT scan is requested.

3.3 Point-source simulations

PDAs for various CsI(Na)-based configurations obtained by the point-source measurements are plotted in Fig. 9. The configurations differ in pixel-pitch. The tracer is ^{99m}Tc. Increasing the pixel-size results in an improved PDA. Correlation of the PDA with PVR of a configuration is shown in Fig. 10. A higher PDA corresponds to a higher PVR. A regression line is also fitted to the data. As the PVR increases, the PDA also improves.

Similar to the pencil-beam study, a higher PDA value would be obtained by using a higher pixel-pitch, and also a same trend was observed. For example, a pixel-pitch of

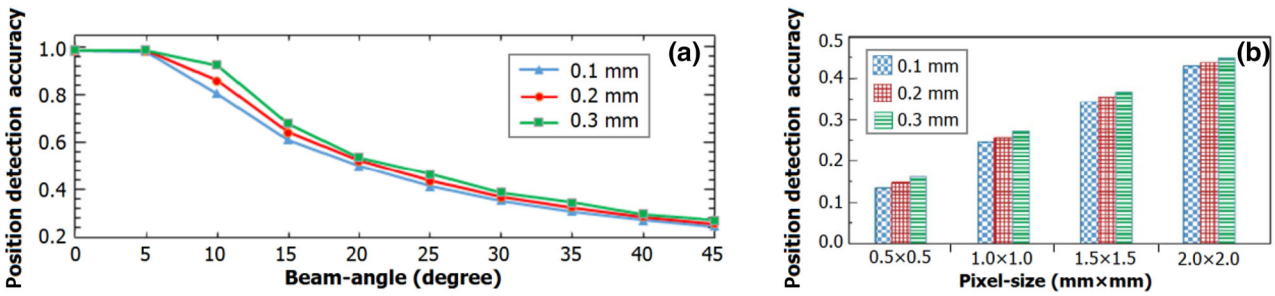

Fig. 7 Position detection accuracy for **a** different beam angles at 1 mm × 1 mm pixel-area and **b** different crystal configurations at 45° incidence, with pixel-gaps of 0.1, 0.2, and 0.3 mm epoxy

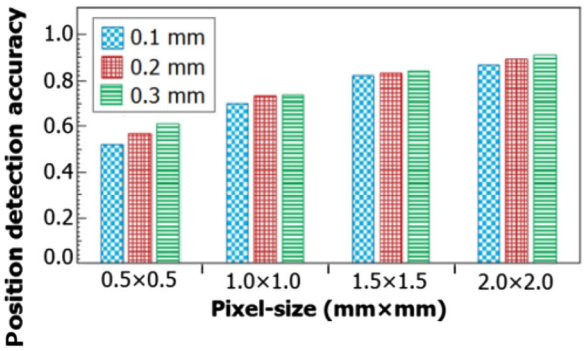

Fig. 9 Position detection accuracy values obtained by flood irradiating of a 11 × 11 CsI(Na) array, with the tracer of ^{99m}Tc

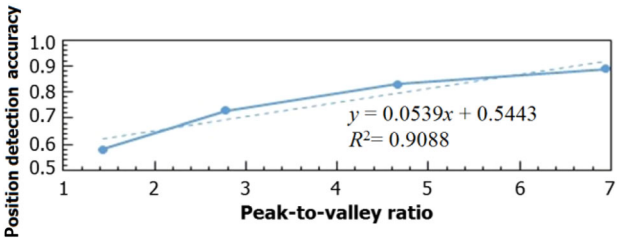

Fig. 10 PDAs versus PVR derived with a ^{99m}Tc point-source, for CsI(Na) crystal configuration

1.2 mm results in a PDA value of 0.73. ICS–P originated from the neighbor crystal elements also contribute to value of these PDAs, as mentioned earlier. From Fig. 10, one can conclude that the PDA linearly correlates the PVR, as expected (R^2 of 0.9). A larger pixel-pitch always provides a higher crystal separation (quantized by the PVR) and also corresponds to a higher PDA. Therefore, the higher the PVR, the higher the PDA. In calculation of the PVRs, the peak and valley heights were averaged. An advantage of a 2.2-mm pixel-pitch (2 mm pixel-size) is a PDA of 0.89, and a PVR of 6.95. Although the PVR is readout dependent (e.g., PS-PMT readout versus SiPM one), the increasing trend is the same.

4 Conclusion

In this work, CI was assessed for various configurations using a dedicated MC platform, GATE. Current trends in medical imaging and ever increasing needs for high spatial resolution in preclinical SPECT imaging mandate to quantify those parameters limiting spatial resolution of the images in order to be incorporated in the reconstruction algorithms.

GATE-provided results show that the ICS–P can cause inaccurate signal positioning and then has a deteriorative impact on CI in SPECT scanners with pixelated crystal. Nonetheless, a higher pixel-size and gap automatically lead to a greater crystal performance, but at the expense of down data sampling resulting in poorer image spatial resolution. The optimum crystal configuration should be then chosen from the well-known PDA-to-resolution tradeoff. It is also concluded that the most rigorous variation of PDA quantity occurs for pixel-size compared to epoxy gap.

On the other hand, spatial resolution of pinhole (or other magnifying) collimators is usually specified and reported at central axis of the collimator, the axis perpendicular to the crystal's face. At edges of the FOV, spatial resolution considerably degrades due to a high ICS–P occurred for oblique projections, commonly referred as the parallax artifact. Therefore, the standard PDA-to-resolution optimization should be addressed, subjecting a minimum acceptable value of the PDA (for example, 0.5 as a rule of thumb), when a pinhole (or slit-hole) collimation is desired. Practically speaking, a threshold value of 0.5 seems to be acceptable for routine preclinical SPECT imaging studies. However, it is up to the decision maker to set an appropriate threshold based upon imaging task. Our future work is to model such effects in system matrix of the HiReSPECT scanner in order to correct the image for the parallax artifact.

References

1. S.R. Meikle, P. Kench, M. Kassiou et al., Small animal SPECT and its place in matrix of molecular imaging technologies. Phys. Med. Biol. **50**, 45–61 (2005). doi:10.1088/0031-9155/50/22/R01
2. F.J. Beekman, B. Vastenhouw, Design and simulation of a high-resolution stationary SPECT system for small animals. Phys. Med. Biol. **49**, 4579–4592 (2005). doi:10.1088/0031-9155/49/19/009
3. M.T. Madsen, Recent advances in SPECT imaging. J. Nucl. Med. **48**, 661–673 (2007). doi:10.2967/jnumed.106.032680
4. H. Zaidi, Recent developments and future trends in nuclear medicine instrumentation. Z. Med. Phys. **16**, 5–17 (2006). doi:10.1078/0939-3889-00288
5. Y. Shao, S.R. Cherry, S. Siegel et al., A study of inter-crystal scatter in small scintillator arrays designed for high resolution PET imaging. IEEE Trans. Nucl. Sci. **43**, 1938–1944 (1996). doi:10.1109/23.507250
6. M. Rasouli, M.R. Ay, A. Takavar et al., The influence of inter-crystal scattering on detection efficiency of dedicated breast gamma camera: a Monte Carlo study, in *4th European Conference of the International Federation for Medical and Biological Engineering*, vol 22 (2009), pp. 2451–2454. doi:10.1007/978-3-540-89208-3_588
7. F. Adibpour, M.R. Ay, S. Sarkar et al., Quantification of inter-crystal scattering and parallax effect in pixelated high-resolution small-animal gamma camera: a Monte Carlo study, in *5th Kuala Lumpur International Conference on Biological Engineering*, vol 35 (2011), pp. 708–711. doi:10.1007/978-3-642-21729-6_172
8. N. Zeraatkar, M.R. Ay, P. Ghafarian et al., Monte Carlo-based evaluation of inter-crystal scatter and penetration in the PET subsystem of three GE Discover PET/CT scanners. Nucl. Instrum. Methods Phys. Res. A **669**, 508–514 (2011). doi:10.1016/j.nima.2011.07.049

9. N. Ghazanfari, S. Sarkar, G. Loudos et al., Quantitative assessment of crystal material and size on the performance of rotating dual-head small-animal PET scanner using Monte Carlo modeling. Hell. J. Nucl. Med. **15**, 33–39 (2012)
10. H. Zaidi, Relevance of accurate Monte Carlo modeling in nuclear medical imaging. Med. Phys. **26**, 574–608 (2000). doi:10.1118/1.598559
11. S. Jan, G. Santin, D. Strul et al., GATE: a simulation toolkit for PET and SPECT. Phys. Med. Biol. **49**, 4543–4561 (2004). doi:10.1088/0031-9155/49/19/007
12. V. Moji, N. Zeraatkar, M.H. Farahani et al., Performance evaluation of a newly developed high-resolution, dual-head animal SPECT system based on the NEMA NU1-2007 standard. J. Appl. Clin. Med. **15**, 267–287 (2014). doi:10.1120/jacmp.v15i6.4936
13. S. Sajedi, N. Zeraatkar, V. Moji et al., Design and development of a high resolution animal SPECT scanner dedicated for rat and mouse imaging. Nucl. Instrum. Methods Phys. Res. A **741**, 169–176 (2014). doi:10.1016/j.nima.2014.01.001
14. N. Zeraatkar, S. Sajedi, M.H. Farahani et al., Resolution-recovery-embedded image reconstruction for a high resolution animal SPECT system. Phys. Med. **30**, 774–781 (2014). doi:10.1016/j.ejmp.2014.05.013
15. M.J. Berger, J.H. Hubble, S.M. Seltzer et al. XCOM: Photon Cross Sections Database. http://physics.nist.gov/PhysRefData/Xcom/Text/XCOM.html
16. G.F. Knoll, *Radiation detection and measurement*, 4th edn. (Wiley, New York, 2010), pp. 223–274